Molecular Dynamics of Poly(benzylphenyl ether) Dendrimers: Effects of Backfolding on Förster Energy-Transfer Rates

Wilfredo Ortiz, Adrian E. Roitberg, and Jeffrey L. Krause*

University of Florida, Quantum Theory Project, P.O. Box 118435, Gainesville, Florida 32611-8435

Received: December 23, 2003; In Final Form: April 15, 2004

We present the results of structural studies of poly(benzylphenyl ether) dendrimers (PBPE dendrimers) using classical molecular dynamics simulations. Specifically, we focus on four generations of PBPE dendrimer at 298 K. Our objectives are to calculate donor/acceptor distances and Förster energy-transfer rates as a function of dendrimer generation. Analyses of the trajectories from molecular dynamics simulations provide information about the radius of gyration and atomic and phenyl group density distributions in generations one through four of the dendrimer. Several different methods for computing rate constants are discussed. The methods include various estimates of average donor/acceptor distances and direct exponential fits to simulated rise-time data. The results can be correlated with observed photophysical properties of dendrimers in related systems containing donor/acceptor pairs. We demonstrate that the wrapping of peripheral groups to the core of the dendrimer leads to very short donor/acceptor distances that dominate the energy-transfer rates.

I. Introduction

Dendrimers are macromolecules that emanate from a central core in a regular, highly branched geometry.[1−7] Impressive advances in synthetic techniques have made it possible to create a large variety of dendrimers, functionalized or decorated in numerous ways.[5] In fact, synthetic schemes have advanced to the point that design strategies can be applied reliably to target dendrimers as biochemicals or pharmaceuticals or highly selective cavities in which novel photochemistry can occur.[5,7] Particularly exciting is the possibility that dendrimers might be produced that mimic biological function, such as enzymatic catalysis or light harvesting.[3,5,7] Dramatic progress has already been made toward these goals.

Direct structural information about dendrimers is difficult to obtain, mainly because they crystallize poorly.[5] However, many indirect techniques have now been developed and are applied routinely in the laboratory to provide detailed information about the structure and function of dendrimers in solution.[2,6,8] One tool that can be used to guide and interpret experiments is computer simulation. Several groups have now shown that such simulations provide data that can be compared directly to experiment.[9−20]

The subject of this study is the Fréchet-type dendrimer poly(benzylphenyl ether) (PBPE).[21] The core unit of the dendrimer consists of a 1,1,1-tris (4′-hydroxyphenyl)-ethane molecule. The repeat units are 3,5-dihydroxybenzyl alcohol molecules, and the terminal units are benzyl groups. Figure 1 shows the core, repeat, and terminal units, and Figure 2 shows 2D sketches of the first four generations of the dendrimer. Following the nomenclature developed in ref 18, capital letters (G_1, G_2, G_3, and G_4) are used to denote the generation of the dendrimer, and lowercase letters (g_1, g_2, g_3, and g_4) are used to label the repeat units within each generation. Hence, G_1 contains only g_1, but G_4 contains g_1, g_2, g_3, and g_4. Note that in this work we do not consider explicit donor and acceptor groups attached to the core and periphery of the dendrimer. Our aim is to identify general structural trends, which will be modified somewhat by the specific moieties used to terminate the dendrons or from which the dendrons are initiated.

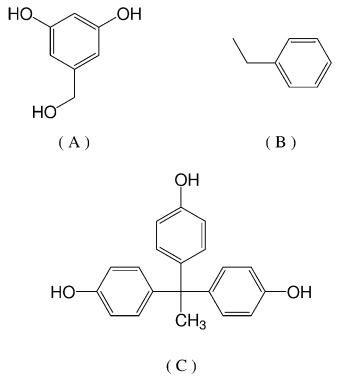

Figure 1. Constituents of the PBPE dendrimers: (A) repeat unit, (B) terminal unit, and (C) core.

In this work, we present the results of classical molecular dynamics simulations of PBPE dendrimers. The structural properties considered are the radius of gyration, root-mean-square deviations, and atomic and phenyl group density profiles. We show that these structural data compare well with previous experimental and theoretical studies. The structural information obtained from the simulations is used to calculate rate constants for energy transfer within the Förster[22] framework. Several possible methods for computing the rate constants are discussed in the context of recent photochemical experiments on related systems.[23−26]

The structural and dynamical information presented in this paper is derived from simulations of single molecules. Each generation has a specific number of donor groups (6 for G_1, 12 for G_2, 24 for G_3, and 48 for G_4), all of which can contribute to the energy-transfer process. As a result, a distribution of rates is determined in the simulations and observed in the experiments. The challenge, as described below, is to correlate the detailed theoretical results with the observed experimental data.

* To whom correspondence should be addressed. E-mail: krause@qtp.ufl.edu.

10.1021/jp0379998 CCC: $27.50
Published on Web 05/20/2004

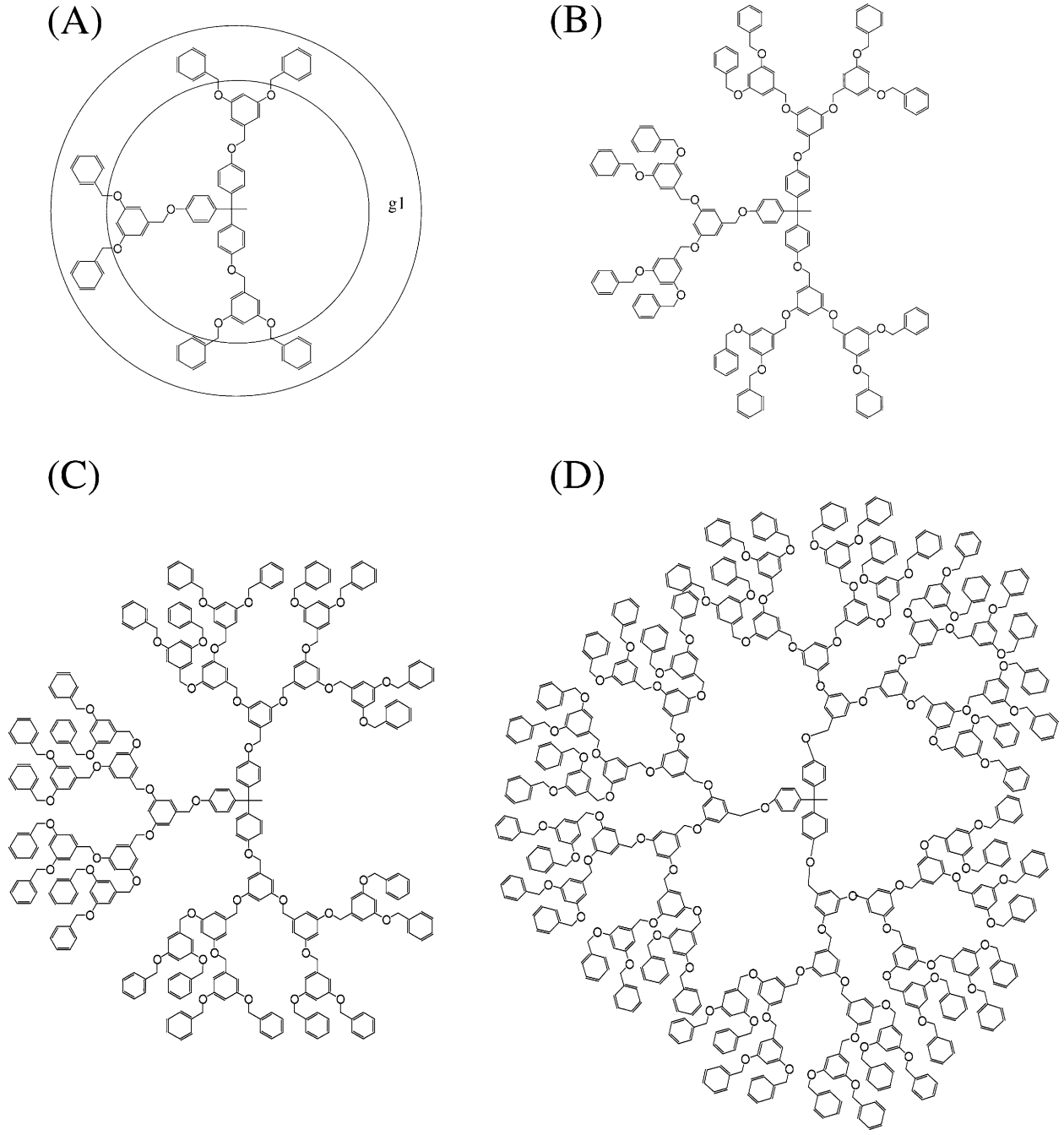

Figure 2. Two-dimensional sketches of the PBPE dendrimers analyzed in this work.

II. Method

The simulations described in this work were performed using the Discover module of Cerius2 from Accelrys Inc.[27] The initial structures were obtained using the sketch tool within Cerius2. A conjugate gradient algorithm was used to minimize the energy of the initial structures. Molecular dynamics (MD) simulations of the energy-minimized structures were performed within the canonical ensemble (*NVT*) at fixed temperatures. The temperature was controlled using the Nosé−Hoover method,[28] and the trajectories were integrated using the velocity Verlet algorithm.[29] The initial structures were equilibrated for 500 ps, followed by 1000 ps of simulation using a time step of 1.0 fs. One frame was saved per picosecond. The data analysis used only the post-equilibrium dynamics.

The force field used in the simulations was PCCF, which has been parametrized to treat polymers and organic materials.[30−32] The main feature of this force field that is important for this system is the flexibility to treat electron delocalization in aromatic rings, which are the essential component of the repeat units in PBPE dendrimers. The electrostatic interactions were modeled using point charges, with the cutoff for the electrostatic and van der Waals interactions fixed at 9.5 Å. The results presented below were tested extensively with additional force fields (Dreiding,[33] MM+,[34] and MM3[35]), longer equilibration and simulation times, and simulated annealing with various annealing schemes. In particular, we found that long equilibration and run times were critical to obtain reliable, converged results. We are confident that the results presented here are valid to within the inherent statistical uncertainty of molecular dynamics.

III. Results and Discussion

The data from the molecular dynamics simulations can be analyzed to extract a variety of structural information. We

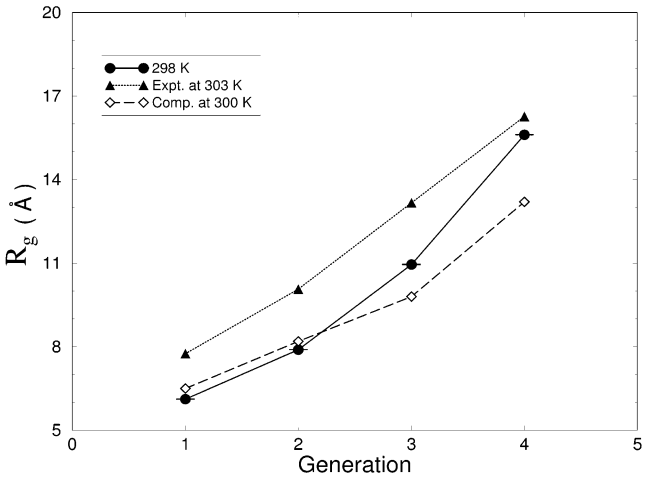

Figure 3. Computed radius of gyration for generations one through four of the PBPE dendrimer (●) compared to experiment[38] (▲) and to the computational results of Naidoo et al.[18] (◊).

calculated the radius of gyration, R_g, to characterize the structural dimension of the PBPE dendrimers. The average radius of gyration is defined as

$$\overline{R_g} = \frac{1}{N_C}\frac{1}{N_{atm}}\sum_{j=1}^{N_C}\sum_{i=1}^{N_{atm}}|r_i - r_c| \qquad (1)$$

where N_{atm} is the total number of atoms, N_C is the total number of configurations, or snapshots, r_i represents the atomic coordinates, and r_c represents the coordinates of the center of mass. A related quantity often measured in experiments is the hydrodynamic radius, which is related to R_g (for a simple, unsolvated sphere)[36,37] by

$$R_g = \left(\frac{3}{5}\right)^{1/2} R_h \qquad (2)$$

The radius of gyration for the first four generations of the PBPE dendrimers is shown in Figure 3. As expected, R_g increases smoothly with generation. If the data are replotted as a function of the number of repeat units (12, 24, 48, and 96 phenyl rings for generations one through four), then the graph is nearly linear. This behavior is an indication that the dendrimers are globular (as shown in Figure 4) with a rather solid, central core. Given the topology of the dendrimeric structure, this can happen only if significant backfolding of the terminal groups and intermingling with intermediate and central groups occur. We shall return to this point below.

The computed radii of gyration agree well with previous calculations.[18] However, as can be seen in Figure 3, they agree at best qualitatively with experiment.[38] The main reason for the discrepancy between theory and experiment is the absence of a solvent in the MD simulations. The experiments were performed in a nonpolar solvent (THF), in which the dendrimers are readily soluble, but the MD simulations were performed in vacuo. In the experiments, the interaction of the solvent with the dendrimers leads to slightly more open structures than those seen in the simulations. Previous work[12] on dendrimers with solvent effects of varying quality showed the same general features

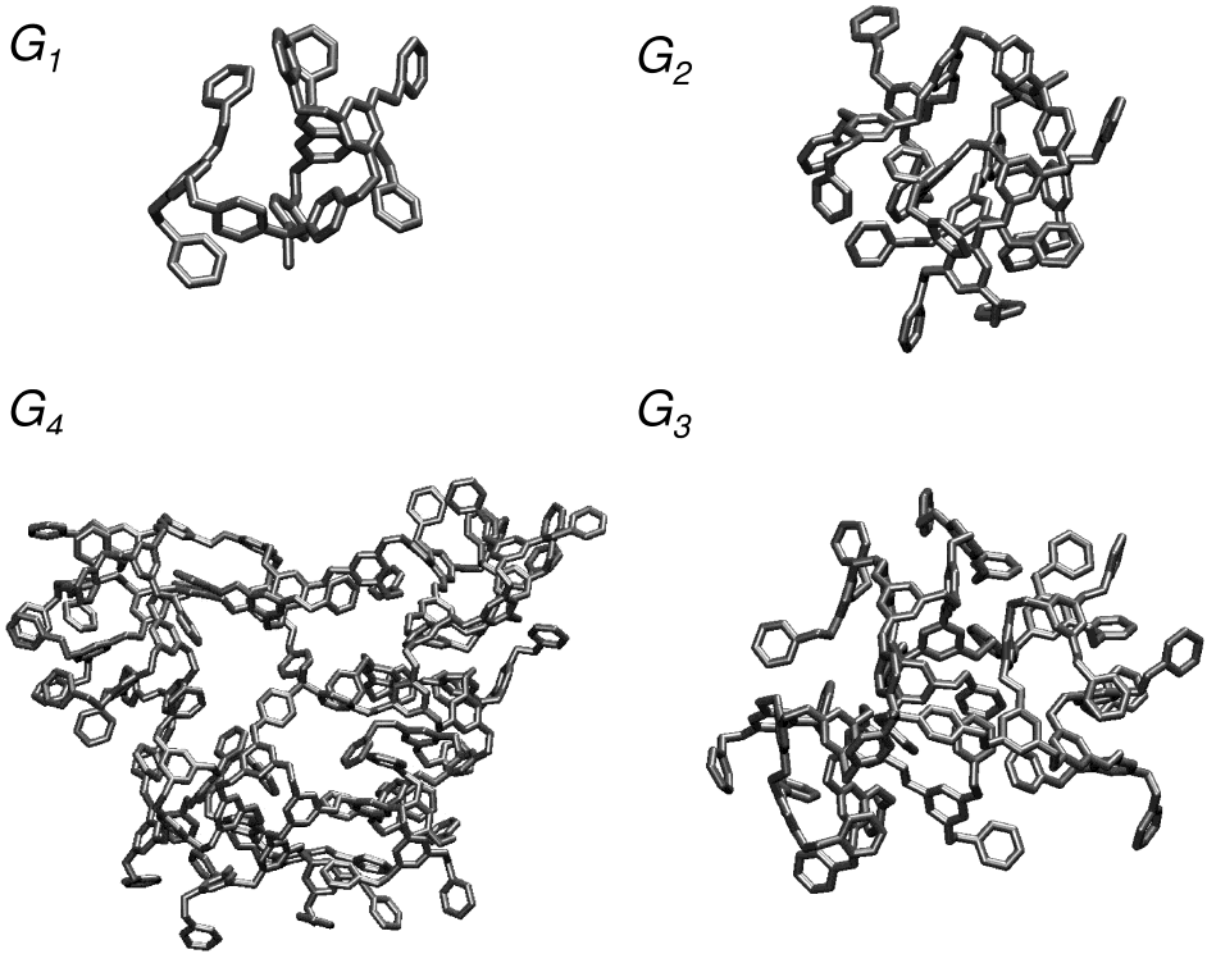

Figure 4. Snapshots of the PBPE dendrimers as obtained from molecular dynamics simulations.

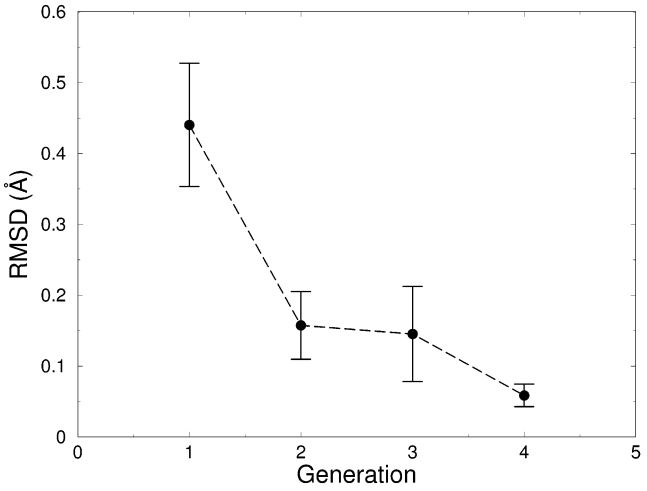

Figure 5. Root-mean-square displacement (rmsd) of the core atoms averaged over time as a function of generation.

observed in our work. In particular, ref 12 showed that the addition of a nonpolar solvent modified the quantitative predictions of the simulation but not the qualitative trends.

Another possible reason for the disagreement with experiment is the deviation from the approximation (unsolvated, perfect sphere) expressed in the relationship between R_g and R_h in eq 2. Note that the initial open structures in the simulations have R_g values ranging from 10 Å for G_1 to 20 Å for G_4, indicating considerable folding in the simulations and less folding in the experiments. Future work will include explicit solvent molecules and will analyze in detail the influence of the solvent−solute interactions on the structural and photophysical properties of dendrimers.

Another question that can be addressed by the simulations is the extent to which attaching dendrons of various lengths affects the core of the dendrimer. Figure 5 shows the root-mean-square displacement (rmsd) of the core atoms (as defined in Figure 1C) as a function of generation at 298 K. We see that the fluctuations of the core atoms are somewhat larger in the smaller generations than in the larger generations, though none of the deviations are significant. A possible explanation for this behavior is the strain in the core in the higher generations. Steric effects caused by the longer branches may hinder movement within the core.[15,39] An alternative explanation that ascribes the stiffness to an extended core structure, rather than steric effects, has also been proposed.[11,12]

To investigate further the extent and effects of backfolding, we calculated atomic and monomer density profiles. The atomic density profiles are computed in a spherical shell and averaged over time (1000 ps) using the following equation,

$$\overline{\rho(R)} = \frac{4\pi}{3N_C[(R+\Delta R)^3 - R^3]}\sum_{i=1}^{N_C} n_i \qquad (3)$$

where n_i is the number of atoms within a spherical shell of radius R and thickness ΔR at a particular time during the simulation. No distinction is made between carbon and oxygen atoms. Hydrogen atoms are excluded from the calculation. The thickness of the shell is chosen to be 0.5 Å.

Figure 6 shows $\overline{\rho(R)}$ for generations one through four of the PBPE dendrimer at 298 K. The atomic density calculation displays five prominent peaks, evident up to 5.5 Å from the reference atom at the center of the core structure. Within the resolution of this Figure, the atomic densities for all four

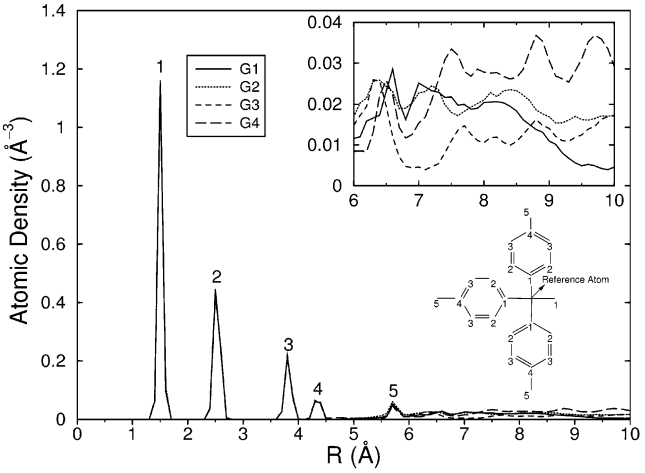

Figure 6. Atomic densities, $\rho(R)$, for generations one through four of the PBPE dendrimer as a function of the distance from the core. The insets show the behavior at larger distances from the core and the reference atoms in the core of the PBPE dendrimer.

generations are nearly the same. This is not surprising because the densities at small radii are dominated by the atoms in the core. The peaks in the atomic density profile correspond to the atomic detail of the core structure, and the distances at which they appear can be correlated to core atoms.

The 2D dendrimer sketched in Figure 6 is labeled with numbers corresponding to peaks in the atomic density plots. The average distances from the reference atom in the 2D sketch in Figure 6 agree well with the locations of the peaks in the atomic density plots. This result is consistent with the rmsd data presented above. For example, the sharp, narrow peaks in Figure 6 occur at small values of rmsd, indicating small fluctuations. Though the rmsd data are somewhat generation-dependent, the variations are within the interval, ΔR, over which the atomic densities are averaged. We also find that the peaks are nearly temperature-independent over the range of 50 to 373 K. These results establish clearly that the atomic density up to 5.5 Å from the core is generation- and temperature-independent.

The inset in Figure 6 reveals the differences in the atomic densities at distances far from the core. At 6 Å from the core, the atomic density remains nearly generation- (and temperature-) independent. At 10 Å from the core, however, generation four has a distinctly higher density than that in the other generations, which is a possible indication of backfolding. Previous theoretical and experimental work has shown similar changes in various properties of G_4.[25,26,40] These changes may be due to site-isolation effects caused by a higher atomic density surrounding the core.[7]

Another way to investigate the extent of backfolding in PBPE dendrimers is to examine the location of the terminal phenyl groups. Figure 7 shows the densities for the terminal phenyl groups averaged over 1000 ps for G_1 through G_4. An examination of the terminal phenyl group densities reveals several trends. The number of terminal groups doubles with each generation, so the phenyl groups are spread over an increasingly large volume. The phenyl group densities move generally to larger distances as the generation increases, indicating considerable flexibility in the dendrimeric structure. However, the distributions also becomes significantly broader as a function of generation. Note in Figure 7 that g_4 in G_4 has a high density at about 9 Å. This is a strong indication of backfolding. In the extended 2D structure for G_4, the terminal phenyl groups are 30 Å from the core. The data in Figure 7 are in excellent agreement with previous studies[9−12,15,18] and in complete

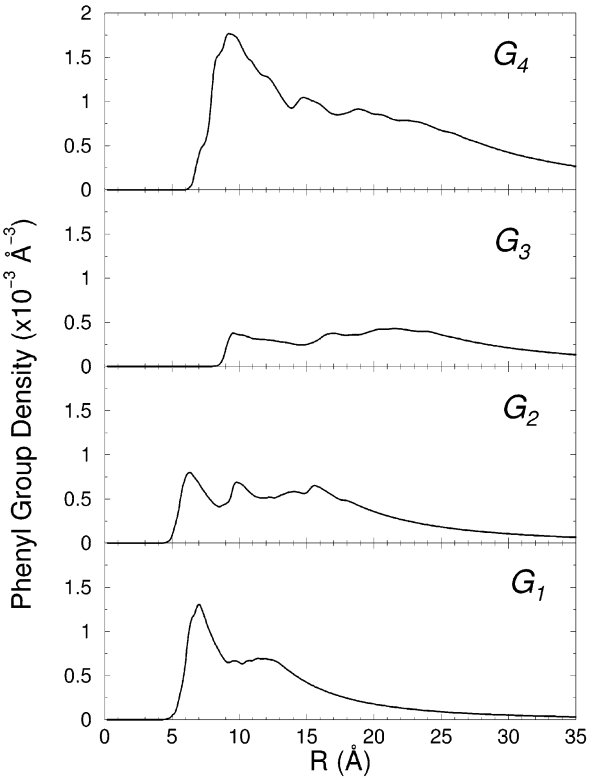

Figure 7. Densities for the terminal phenyl groups in generations one through four of the PBPE dendrimer. From top to bottom: g_4 in G_4, g_3 in G_3, g_2 in G_2, and g_1 in G_1.

disagreement with early work by de Gennes and Hervet,[14] which predicted essentially hollow dendrimers with most of the atomic density on the periphery.

The structural data discussed above can be used as a guide to interpret several recent experiments. One example is the energy-transfer experiments by Fréchet and Fleming.[23,24] In these experiments, poly(aryl ether) dendrimers, which are similar in structure to the PBPE dendrimers discussed here, were labeled with laser dyes to act as energy donors (at the periphery of the dendrimer) and energy acceptors (at the core of the dendrimer). The structure of the repeat units in the dendrimer ensured that energy transfer occurred via Coulombic coupling between the chromophores and not via superexchange or other through-bond mechanisms. In the initial experiment, the decay of the acceptor fluorescence was measured with pump−probe spectroscopy. This experiment demonstrated clearly that the functionalized dendrimers act as highly efficient light-harvesting antennae. In a subsequent experiment with improved time resolution, the authors measured the rise time of the acceptor fluorescence, which can be directly related to the rate constant for energy transfer.

To interpret the experimental data, the experimental groups used the Förster model,[22] which is appropriate for the case of long-range Coulombic interaction of point dipoles. In this model, the Coulombic coupling is calculated using the ideal dipole approximation (IDA). That is, the transition density is assumed to be simply the transition dipole. In the Förster model, the rate constant for energy transfer is given as

$$k_{ET} = C\left(\frac{\kappa^2 \phi_D J}{n^4 \tau_D R^6}\right) \tag{4}$$

where $C = 9000\ \ln(10)/(128\pi^5 N_A)$, N_A is Avogadro's number, κ^2 is the orientation factor of the transition dipole moments, ϕ_D is the donor quantum yield, J is the overlap integral of the donor emission spectrum with the acceptor absorption spectrum, n is the index of refraction of the solvent, τ_D is the donor lifetime in the absence of the acceptor, and R is the distance between the donor and acceptor groups.

The Förster model has the advantage that all of the variables in the expression except R are either constants or can be measured experimentally. However, because the expression depends on the sixth power of R, an accurate determination of R is crucial. To model their data, the authors of the experimental work used an average value of R determined from a conformational search of molecular models of the dendrimer structure in the absence of solvent. Using this method, they obtained excellent agreement with experiment.[23,24]

One point noted in the previous work was that the rise-time data required, in general, multiple exponentials to fit the data adequately. The authors ascribed this observation to the inhomogeneity of the energy-transfer rates due to a distribution of donor/acceptor distances.[23,24] From a biexponential fit of the rise-time data, they extracted an average rise time, which was then converted to a rate constant.

In this work, we apply a similar procedure to compute rate constants using data extracted from the simulations discussed above. Because the simulations have complete knowledge of the distances of all peripheral groups from the core, we can examine the validity of assuming an average rise time and the factors leading to the observed multiexponential rise times.

In the calculations discussed below, we chose the following values for the parameters in eq 4: $\kappa^2 = {}^2/_3$,[41] $\phi_D = 0.053$,[42] $J = 1.2 \times 10^{-13}$ cm^6/mol, $n = 1.0$,[43] and $\tau_D = 10$ ns.[44] These values assume that the "acceptor" is 1,1,1-tris (4-hydroxyphenyl)-ethane and the "donor" is a terminal phenyl group. To calculate J, we obtained the donor emission spectrum from ref 42 and calculated the acceptor absorption spectrum using ZINDO.[45] In choosing these values, we are not suggesting that PBPE is *itself* a good candidate in which to observe energy transfer but are simply establishing an unambiguous model.

The remaining parameter in eq 4 is R, the distance between the donor and the acceptor. A variety of methods exist for calculating this parameter. The simplest is to use the radius of gyration. Another is to choose an average value of R by calculating the average donor−acceptor distance in a given (computer-generated) structure and then averaging over many such structures. The most consistent method (within the MD framework) is to calculate the contribution from each terminal group in a given structure and then average over a number of configurations, as in

$$\overline{k_{ET}} = \frac{A}{N_C N_T} \sum_{j=1}^{N_C} \sum_{i=1}^{N_T} \frac{1}{R_{ij}^6} \tag{5}$$

where $A = C\kappa^2\phi_D J/(n^4\tau_D)$, N_C is the number of configurations in the average, N_T is the number of terminal groups, and R is the distance between the donor and acceptor groups. Note that κ^2, in principle, is different in each configuration. In accord with the usual experimental assumption, we have kept κ^2 fixed at ${}^2/_3$.

The donor/acceptor values of R for the three methods discussed above are presented in Table 1. If we use the radius of gyration as our measure of the donor/acceptor distance, then we are assuming that the dendrimer is a perfect sphere with the acceptor group at the center of mass of the sphere and the donor groups on the surface. In fact, the calculation of the distance between the acceptor groups and the center of mass of the

TABLE 1: Calculated Donor/Acceptor Distance by Three Methods, as Described in the Text[a]

generation	R_g	$\bar{R}$	$\overline{(1/R^6)}^{(-1/6)}$
G_1	6.12 (±0.05)	9.52 (±0.28)	7.25 (±0.89)
G_2	7.90 (±0.07)	12.91 (±0.15)	8.39 (±0.77)
G_3	11.07 (±0.07)	18.68 (±0.16)	13.57 (±0.73)
G_4	15.61 (±0.10)	18.04 (±0.10)	10.93 (±0.76)

[a] Numbers in parentheses are standard deviations. Distances and standard deviations are in angstroms.

TABLE 2: Calculated Rate Constants for Energy Transfer by Four Methods, as Described in the Text[a]

generation	$k_{ET}(R_g)$	$k_{ET}(\bar{R})$	$\overline{k_{ET}(R)}$	k_{ET}^{fit}
G_1	718.0	50.7	260.5	26.7
G_2	155.0	8.1	108.4	4.7
G_3	20.5	0.9	6.0	0.6
G_4	2.6	1.1	22.1	0.5

[a] Rate constants are in units of 10^{10} s^{-1}.

dendrimer indicates that the core of the dendrimer is displaced by 4 to 10 Å from the center of mass. Consequently, the radius of gyration presents an incomplete description of the location of the donor groups.

The other two methods listed in the Table ($\bar{R}$ and $\overline{(1/R^6)}^{(-1/6)}$) provide a better description of the distance between donor and acceptor groups. The trend in the donor/acceptor distance predicted by R_g is different from that of $\bar{R}$ and $\overline{(1/R^6)}^{(-1/6)}$. R_g shows a smooth increase in the donor/acceptor distance as a function of generation. This trend is not observed in $\bar{R}$ or $\overline{(1/R^6)}^{(-1/6)}$. Histograms of the donor/acceptor distances show that some terminal groups in G_4 are closer to the core than any terminal group in G_3. This effect is more pronounced in $\overline{(1/R^6)}^{(-1/6)}$ and is not observed in R_g.

The rate constants for energy transfer for the three methods discussed above are displayed in Table 2. These rate constants were obtained using eq 4, with the donor/acceptor distances in Table 1. The last column in the Table, k_{ET}^{fit}, is the average rate constant calculated from a two-exponential fit to simulated rise-time data (as described below). As expected, the rate constants computed from the radius of gyration data are in considerable disagreement with those from the other two methods ($k_{ET}(\bar{R})$ and $\overline{k_{ET}(R)}$). The rate constants calculated with R_g are not only incorrect quantitatively but fail to predict the qualitative trend. Note, in particular, that the more accurate methods predict a higher rate constant for G_4 than for G_3, whereas R_g predicts the opposite.

Although the rate constants calculated with various average values of R are informative, the use of an average R represents a highly coarse-grained approach to the problem. The data obtained in the MD simulations can be processed in many ways to gain insight into the dynamics. As an example, Figure 8 shows a histogram of the donor/acceptor distances in G_1 of the dendrimer. The histogram has a bimodal distribution, indicating that the most probable donor/acceptor distance is localized in two different regions, at distances of 6 and 11 Å from the core. This plot shows that not all terminal groups are localized on the surface of the molecule (as would be implied from the R_g data).

Because the rate constant depends sensitively on the distance between the donor and acceptor, a strong correlation is expected between the distribution of donor/acceptor distances and decay times. Figure 9 shows the distribution of decay times for the

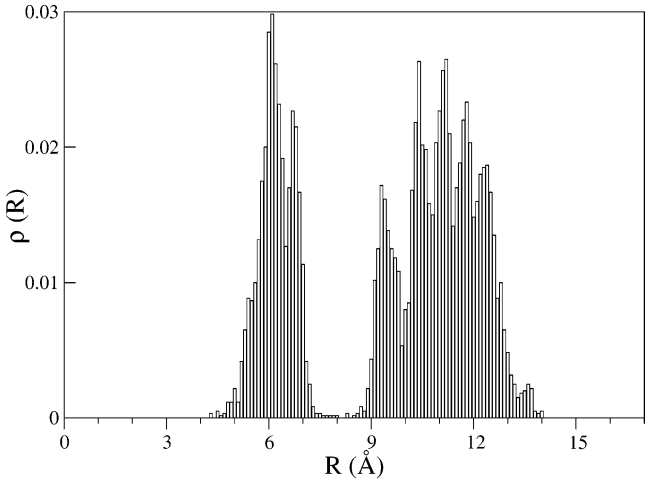

Figure 8. Histogram of the donor/acceptor distances for all terminal groups in G_1.

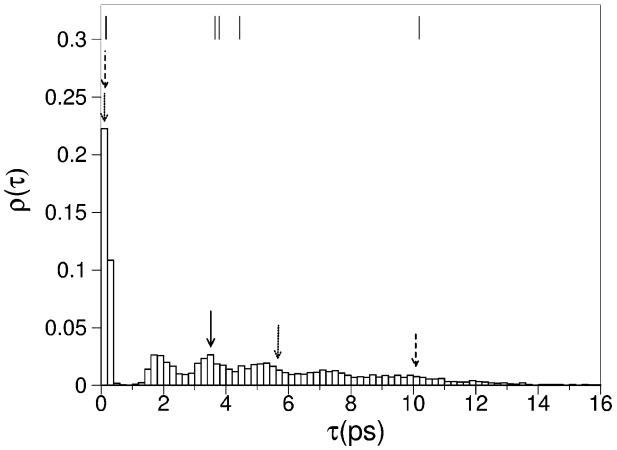

Figure 9. Histogram of the decay times for all terminal groups in G_1. The arrows indicate the τ_i components of the exponential fits to the simulated rise-time data. The solid arrow is from the one-exponential fit. The dotted arrows are from the two-exponential fit. The dashed arrows are from the three-exponential fit. The solid bars are the averaged decay times from each of the six terminal groups.

TABLE 3: Calculated Rate Constants for Energy Transfer and Decay Times for the Six Terminal Groups in G_1

terminal group	$\overline{k_{ET}(R)}$ (10^{10} s^{-1})	$\bar{\tau}$ (ps)
T_1	652.87	0.15
T_2	600.43	0.17
T_3	27.39	3.65
T_4	26.43	3.78
T_5	22.50	4.44
T_6	9.81	10.19

donor groups in G_1. The decay times were calculated from the distribution of distances presented above (Figure 8) with the Förster model. The Figure shows a bimodal distribution that correlates with Figure 8. Note, in Figure 9, a narrow distribution with fast (subpicosecond) time scales and a second broader distribution that ranges from 2 to 14 ps. If we examine the contribution from each terminal group, we see that two out of six terminal groups are responsible for the fast decay times, with the remainder distributed between 2 and 14 ps.

Table 3 shows the rate constants and corresponding decay times from the average distances between donor and acceptor groups in the first generation of the PBPE dendrimer. Note that in G_1 there are six terminal groups, each of which gives rise to an average decay time, and rate constant. The six decay times

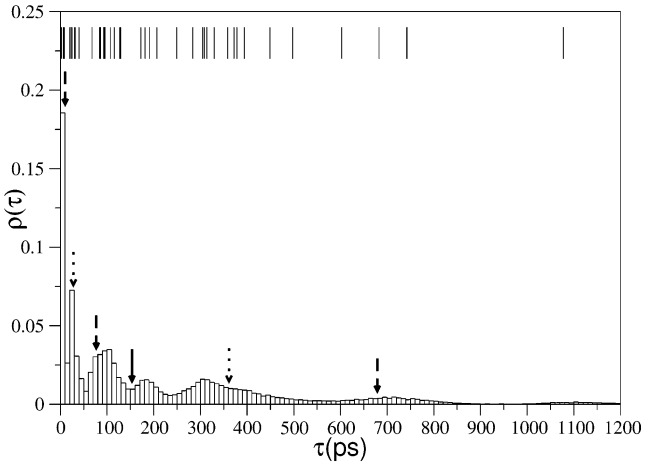

Figure 10. Histogram of the decay times for all 48 terminal groups in G_4. The arrows indicate the τ_i components of the exponential fit to the simulated rise-time data. The solid arrow is from the one-exponential fit. The dotted arrows are from the two-exponential fit. The dashed arrows are from the three-exponential fit. The solid bars are the averaged decay times from each of the 48 terminal groups.

TABLE 4: Parameters for a One-Exponential Fit to Simulated Rise-Time Data as a Function of Generation

generation	A_1	τ_1 (ps)
G_1	1.00	3.20
G_2	1.00	18.30
G_3	1.00	154.17
G_4	1.00	159.30

obtained in this way are plotted with small solid lines at the top of Figure 9. The rate constants are distributed into three time scales: ~0.20, ~4, and ~10 ps. The fast decay times originate from terminal groups close to the core (within a few angstroms) and the slow decay times from terminal groups at greater distances.

The distribution of decay times in the fourth generation (Figure 10) is broader because the dendritic branches in G_4 are longer than in G_1. Consequently, some terminal groups in G_4 are much further away from the core than in G_1 and produce very slow decay times (~1200 ps). However, there are also terminal groups with decay times of the same magnitude as in G_1 (<1 ps). These decay times are possible only because of the backfolding of terminal groups to the core.

Another way to look at the data is to use the rate constants calculated above to simulate the experimental rise times using the following equation:

$$S(t) = 1 - \frac{1}{N_T}\sum_{i=1}^{N_T} e^{-k_{ET}^{i}t} \qquad (6)$$

Then, as in the experiments, the signal can be fit to a sum of exponentials,

$$S(t) = 1 - \sum_j A_j e^{-t/\tau_j} \qquad (7)$$

to obtain the energy-transfer coefficients and weights. From these data, average energy-transfer times and rate constants can be derived. In principle, if the signal for G_4 were fit with 48 exponentials, then the result would be in perfect agreement with the value calculated above. In practice, fits with more than two or three exponentials are not significant numerically.

In Tables 4−6, we show the computed parameters for the one-, two-, and three-exponential fits to the simulated rise-time data as a function of generation. As expected, the decay time obtained from the one-exponential fit increases as the generation increases. For the two-exponential fit, the slower time component (τ_2) is also generation-dependent, but the fast time component (τ_1) increases with generation up to G_3 and then decreases for the fourth generation. Moreover, the fast time component increases in weight as a function of generation.

TABLE 5: Parameters for a Two-Exponential Fit to Simulated Rise-Time Data as a Function of Generation

generation	A_1	τ_1 (ps)	A_2	τ_2 (ps)
G_1	0.35	0.25	0.65	5.63
G_2	0.45	3.48	0.55	35.72
G_3	0.46	37.92	0.54	291.69
G_4	0.50	26.60	0.50	369.62

TABLE 6: Parameters for a Three-Exponential Fit to Simulated Rise-Time Data as a Function of Generation

generation	A_1	τ_1 (ps)	A_2	τ_2 (ps)	A_3	τ_3 (ps)
G_1	0.33	0.16	0.50	3.91	0.17	10.07
G_2	0.27	1.24	0.51	17.23	0.22	60.95
G_3	0.17	7.14	0.45	92.38	0.38	362.99
G_4	0.25	3.91	0.40	91.76	0.35	679.77

If we compare the decay times in Table 3 with the components of the three-exponential fit in G_1, we obtain qualitative agreement. In particular, note that the time components in the three-exponential fit are of the same magnitude as the decay times presented in Table 3. In fact, the distribution of six different decay times (due to six terminal groups) fits nearly perfectly with three exponentials ($R^2 = 1.0$).

Figure 9 shows the histogram of decay times for the first generation. The arrows above the histogram represent the τ components of the exponential fits in Tables 4−6. As seen in the Tables, the first generation requires three exponentials to sample the distribution of decay times adequately. In contrast, for the fourth generation the three-exponential fit provides an incomplete description of the distribution of decay times (Figure 10).

One feature captured by the three-exponential fit is the dependence in generation of the slow time component and the absence of this dependence for the fast time component. As the generation increases, the dendritic branches become longer, and the maximum distance of the peripheral groups from the core increases. This would imply that as a function of generation the slow time component should increase. However, the magnitude of the fast time component does not change much as a function of generation because of the wrapping of the terminal groups to the core.

As mentioned above, Table 2 also shows the average energy-transfer rate constants calculated from the synthesized rise-time data. The rate constants obtained from these data are in better agreement with $k_{ET}(\bar{R})$ than with $\overline{k_{ET}(R)}$. Note that the difference in k_{ET} between G_3 and G_4 is larger in $\overline{k_{ET}(R)}$ than in $k_{ET}(\bar{R})$. Given the structural data presented above and the sensitivity of k_{ET} to R (because of the $1/R^6$ dependence in the Förster model), we believe that $\overline{k_{ET}(R)}$ is the correct approach to calculate Förster energy-transfer rates for computer-generated structures. In fact, this method is used in nuclear magnetic resonance (NMR) spectroscopy to obtain the distance between protons in nuclear Overhauser (NOE) experiments.[46]

Conclusions

Using classical molecular dynamics simulations, we studied the structures of four generations of PBPE dendrimers at 298

K. Calculations of the radius of gyration, atomic densities, and phenyl group densities revealed a structure with a rigid, generation-independent core and flexible branches. Considerable evidence of backfolding was displayed, especially in the higher generations. Backfolding is well documented in the literature,[6] but the results here are a clear example of the influence that this effect can have on the dynamics of energy transfer.

We used structural data from the simulations to help interpret recent transient absorption experiments on a related dendrimer. Our results suggest that the method for determining the donor−acceptor distance must be chosen carefully. In fact, it is not at all clear how the "true" energy-transfer rate can be extracted from experimental rise-time data or the relevance of characterizing the energy-transfer process with a single average rate. Similar concerns were expressed in recent experimental work by Kalinin et al.[47] The multiple exponential fits to the fluorescence rise-time data do indeed, as suggested by the experimental data, result from an inhomogeneity in the donor−acceptor distances. In fact, the comparatively rare event of a terminal group wrapping the core dominates the rate constant.

Acknowledgment. We thank Professor V. D. Kleiman for useful discussions and comments. This work was partially supported by the Department of Energy through grant DE-FG02-02ER45995. J.L.K. thanks the Danish−American Fulbright commission for its support on his sabbatical leave in Denmark, where some of this work was completed.

References and Notes

(1) Newkome, G. R.; Moorfield, C. N.; Vögtle, F. *Dendrimers and Dendrons*; Wiley-VCH: Weinheim, Germany, 2001.
(2) *Dendrimers and Other Dendritic Polymers*; Fréchet, J. M. J., Tomalia, D. A., Eds.; John Wiley & Sons: New York, 2002.
(3) Adronov, A.; Fréchet, J. M. J. *Chem. Commun.* **2000**, 1701.
(4) Hearshaw, M. A.; Moss, J. R. *Chem. Commun.* **1999**, 1.
(5) Inoue, K. *Prog. Polym. Sci.* **2000**, *25*, 453.
(6) Bosman, A. W.; Janssen, H. M.; Meijer, E. W. *Chem. Rev.* **1999**, *99*, 1665.
(7) Hecht, S.; Fréchet, J. M. J. *Angew. Chem., Int. Ed.* **2001**, *40*, 74.
(8) Ballauff, M. *Top. Curr. Chem.* **2001**, *112*, 177.
(9) Boris, D.; Rubinstein, M. *Macromolecules* **1996**, *29*, 7251.
(10) Naylor, A. M.; Goddard, W. A., III; Kiefer, G. E.; Tomalia, D. A. *J. Am. Chem. Soc.* **1989**, *111*, 2339.
(11) Mansfield, M. L.; Klushin, L. I. *Macromolecules* **1993**, *26*, 4262.
(12) Murat, M.; Grest, G. *Macromolecules* **1996**, *29*, 1278.
(13) Cagin, T.; Wang, G.; Martin, R.; Goddard, W. A., III; Breen, N. *Nanotechnology* **2000**, *11*, 77.
(14) de Gennes, P. G.; Hervet, H. *J. Phys. Lett.* **1983**, *44*, L351.
(15) Lescanec, R. L.; Muthukumar, M. *Macromolecules* **1990**, *23*, 2280.
(16) Lyulin, A. V.; Davies, G. R.; Adolf, D. B. *Macromolecules* **2000**, *33*, 6899.
(17) Lyulin, A. V.; Davies, G. R.; Adolf, D. B. *Macromolecules* **2000**, *33*, 3294.
(18) Naidoo, K. J.; Hughes, S. J.; Moss, J. R. *Macromolecules* **1999**, *32*, 331.
(19) Tretiak, S.; Mukamel, S. *Chem. Rev.* **2002**, *102*, 3171.
(20) Tada, T.; Nozaki, D.; Kondo, M.; Yoshizawa, K. *J. Phys. Chem. B* **2003**, *107*, 14204.
(21) Hawker, C. J.; Fréchet, J. M. J. *J. Am. Chem. Soc.* **1990**, *112*, 7638.
(22) Forster, T. *Ann. Phys.* **1948**, *6*, 55.
(23) Adronov, A.; Gilat, S. L.; Fréchet, J. M. J.; Ohta, K.; Neuwahl, F. V. R.; Fleming, G. R. *J. Am. Chem. Soc.* **2000**, *122*, 1175.
(24) Neuwahl, F. V. R.; Righini, R.; Adronov, A.; Malenfant, P. R. L.; Fréchet, J. M. J. *J. Phys. Chem. B* **2001**, *105*, 1307.
(25) Jiang, D. L.; Aida, T. *Nature* **1997**, *388*, 454.
(26) Kawa, M.; Fréchet, J. M. J. *Chem. Mater.* **1998**, *10*, 286.
(27) The Cerius2 Discover software package is available from Accelrys Inc.;San Diego, CA 92121.
(28) Hoover, H. *Phys. Rev. A* **1985**, *31*, 1695.
(29) Verlet, L. *Phys. Rev.* **1967**, *159*, 98.
(30) Hwang, M. J.; Stockfisch, T. P.; Hagler, A. T. *J. Am. Chem. Soc.* **1994**, *116*, 2515.
(31) Sun, H. *Macromolecules* **1995**, *28*, 701.
(32) *Force Field-Based Simulations*; Molecular Simulations Inc.: San Diego, CA, 1997.
(33) Mayo, S. L.; Olafson, B. D.; Goddard, W. A., III. *J. Phys. Chem.* **1990**, *94*, 8897.
(34) Allinger, N. L. *J. Am. Chem. Soc.* **1977**, *99*, 8127.
(35) Allinger, N. L.; Yuh, Y. H.; Lii, J.-H. *J. Am. Chem. Soc.* **1989**, *111*, 8551.
(36) Tanford, C. *Physical Chemistry of Macromolecules*; John Wiley & Sons: New York, 1961.
(37) Freifelder, D. *Principles of Physical Chemistry with Applications to the Biological Sciences*; Jones and Bartlett Publishers: Boston, 1985.
(38) Mourey, T. H.; Turner, S. R.; Rubinstein, M.; Fréchet, J. M. J.; Hawker, C. J.; Wooley, K. L. *Macromolecules* **1992**, *25*, 2401.
(39) Meltzer, A. D.; Tirrell, D. A.; Jones, A. A.; Inglefield, P. T.; Hedstrand, D. M.; Tomalia, D. A. *Macromolecules* **1992**, *25*, 4541.
(40) Tanaka, S.; Itoh, S.; Kurita, N. *Chem. Phys. Lett.* **2000**, *323*, 407.
(41) Turro, N. J. *Modern Molecular Photochemistry*; The Benjamin/Cummings Publishing Company, Inc.: Menlo Park, CA, 1978.
(42) Dawson, W. R.; Windsor, M. W. *J. Phys. Chem.* **1968**, *72*, 3251.
(43) Skoog, D. A.; West, D. M.; Holler, F. J. *Fundamentals of Analytical Chemistry*; Saunders College Publishing: Orlando, FL, 1996.
(44) Berlan, I. B. *Energy Transfer Parameters of Organic Compounds*; Academic Press: New York, 1973.
(45) Zerner, M. C. *ZINDO: Quantum Theory Project*; University of Florida: Gainesville, FL, 2001.
(46) Neuhaus, D.; Williamson, M. P. *The Nuclear Overhauser Effect in Structural and Conformational Analysis*; John Wiley and Sons: New York, 2000.
(47) Kalinin, S.; Johansson, L. B.-A. *J. Phys. Chem. B* **2004**, *108*, 3092.